

# Thermodynamics of the disordered Hubbard model studied via numerical linked-cluster expansions

Jacob Park and Ehsan Khatami\*

*Department of Physics and Astronomy, San José State University, San José, California 95192, USA*

(Dated: October 19, 2021)

The interplay of disorder and strong correlations in quantum many-body systems remains an open question. That is despite much progress made in recent years with ultracold atoms in optical lattices to better understand phenomena such as many-body localization or the effect of disorder on Mott metal-insulator transitions. Here, we utilize the numerical linked-cluster expansion technique, extended to treat disordered quantum lattice models, and study exact thermodynamic properties of the disordered Fermi-Hubbard model on the square and cubic geometries. We consider box distributions for the disorder in the onsite energy, the interaction strength, as well as the hopping amplitude and explore how energy, double occupancy, entropy, heat capacity and magnetic correlations of the system in the thermodynamic limit evolve as the strength of disorder changes. We compare our findings with those obtained from determinant quantum Monte Carlo simulations and discuss the relevance of our results to experiments with cold fermionic atoms in optical lattices.

## I. INTRODUCTION

The interplay between electronic correlations and quenched (static) disorder is not well understood. From the experimental point of view, condensed matter experiments aiming at realizing either the Mott transition or Anderson localization in real materials have to worry about the presence of disorder in case of the former, or correlation effects in case of the latter since Coulomb interaction will always be present. For example, the expected first-order Mott transition in phosphorus-doped silicon upon increasing dopants is found to be continuous due to the random distribution of dopants in the so-called Mott-Anderson transition [1]. Experiments of disordered two-dimensional (2D) electron gases done in silicon metal-oxide-semiconductor field-effect transistors [2] find weak localization, but also find several other phenomena, such as a region of linear dependence of resistivity on temperature and a sharp drop in resistivity at low temperatures that may be explained only if one takes into account other factors such as the range of scattering centers, and electronic correlations in cleaner samples. Later studies [3, 4] shed more light on the role of interaction in the metal-insulator transition and quantum criticality in these materials.

The presence of quenched disorder in strongly correlated materials exhibiting unconventional properties also confirms the need to treat disorder and electronic correlations on the same footing in order to be able to describe the complex and competing phases [5, 6]. Recent examples are the interplay of charge density wave order and high-temperature superconductivity in cuprates [7] or the spin liquid behavior in herbertsmithites [8, 9].

Encouraged by an unprecedented control and measurement possibilities in experiments with ultra-cold atomic gasses [10], pure Anderson localization of matter waves

was first realized in 2008, [11, 12] using disorder potentials introduced through laser speckles [13], or a quasi-periodic lattice potential [14] in Bose-Einstein condensates trapped in one dimension. These experiments generated a lot of interest in the community and later inspired the experimental realization of the disordered Bose-Hubbard model [15–17].

Presently, an exciting new frontier is the exploration of many-body localization through the simulation of disordered models in optical lattices [18], and the idea that disorder may in fact help achieve lower temperatures in experiments [19]. In a pioneering work, Kondov et al. [20] studied the Fermi-Hubbard model experimentally in the limit of strong correlations and found that by increasing the interaction strength the system undergoes an insulator to metal transition, and that for larger disorder strengths the onset of the transition is moved to larger interactions. Consistent with many-body localization prediction, there is also a lack of thermally activated conductivity. More recently, out-of-equilibrium properties of the disordered Fermi-Hubbard model in three dimensions (3D) has also been studied across a range of disorder and interaction strengths, where phenomena such as “bad metal” and a disorder-induced pseudogap were observed [21].

While phenomenological theory and approximations can describe some of these observations, the need for reliable exact results of the microscopic model is greater than ever. In light of the great progress made towards our understanding of spin and charge correlations in the clean 2D and 3D Fermi-Hubbard models emulated in optical lattice experiments through cross comparison of results with exact numerical solutions in recent years [22–30], the new progress in preparing and manipulating disordered quantum lattice models calls for highly-precise and readily available numerical solutions of the corresponding models in temperature ranges relevant to experiments.

Among the methods that deal with the disordered Fermi-Hubbard model are the determinant quantum Monte Carlo (DQMC) [19, 31–36], the Monte Carlo

---

\* Corresponding author: ehsan.khatami@sjsu.edu

mean-field approximation [37], the density matrix renormalization group [38, 39], and dynamical mean-field theory (DMFT)-based methods [32, 40, 41] extended to incorporate disorder, such as the statistical DMFT [42], the DMFT+Sigma approach [43, 44], which dresses the local Green's function by an additional approximate self energy due to interactions outside of the DMFT (here, disorder), or the typical-medium dynamical cluster approximation [45, 46], in which the cluster density of states is replaced by its typical value, but the local part of the typical density of states is explicitly separated out and geometrically averaged over disorder configurations. Exact diagonalization with disorder averaging has also been used to study the equilibrium and non-equilibrium properties of the Hubbard models [47, 48].

While these techniques can access low-temperature properties and even explore quantum phase transitions of the disordered Hubbard models, each suffers from one or more limitation that may prevent it from being the ideal candidate for the characterization of the systems studied in optical lattice experiments in some parameter region. The other major issue with methods that take the disorder average randomly is the introduction of statistical errors associated with disorder averaging, which can introduce significant fluctuations in the calculated properties even at intermediate temperatures. The QMC-based methods are also better suited for systems with only weak- to intermediate-strength interactions; as we will see later they can run into technical difficulties in strong-coupling regions of the Hubbard models. Moreover, comparisons to experimental data often requires fast calculations of thermodynamic properties for a wide range of model parameters, temperatures, and densities, something that takes considerable time and computational resources to achieve with methods that do not have access to the full energy spectrum.

In this paper, we use the numerical linked-cluster expansion (NLCE) [49, 50], extended to treat random disorder [51]. The main advantage of the NLCE is the fact that it yields exact finite-temperature results for the Hubbard model *in the thermodynamic limit* (no finite-size or statistical errors). Moreover, similar to ED of finite clusters, one can obtain all the properties for a set of model parameters in a single run on an arbitrarily dense temperature or density grid. The process is fast and allows one to perform a systematic study of thermodynamic properties of the disordered model in 2D and 3D. While highlighting the effectiveness of these features here, it should be noted that the main weakness of the NLCE over most other numerical methods is its limitation in reaching low temperatures; the convergence of the series expansion is typically lost at a finite temperature that in general depends on the model and its parameters.

We separately consider site, interaction, and hopping disorders with a range of strengths and monitor properties such as the average energy, double occupation fraction, heat capacity, entropy and spin correlations as a function of temperature. We find that these properties

are much more sensitive to disorder in the chemical potential than disorder in the onsite interaction strength. At half filling, the former strongly suppresses the magnetic correlations by suppressing moment formation and promotes a state in which particles are localized at sites with significantly lower chemical potential, as evidenced by the enhancement of the fraction of doubly-occupied sites as the temperature is lowered. The bond disorder hinders the NLCE's ability to access low temperatures, however, we find evidence for the formation of dimers on strong bonds at low temperatures. We also present results from the DQMC after disorder realization averaging, which show good agreement with our exact NLCE results and expose the strengths and weaknesses of each method in different parameter regions.

## II. MODELS

We study the Fermi-Hubbard model [52, 53] with random box disorder introduced to its various parameters through the following Hamiltonian:

$$\begin{aligned}
 H = & - \sum_{\langle ij \rangle \sigma} t_{ij} c_{i\sigma}^\dagger c_{j\sigma} \\
 & + \sum_i U_i \left( n_{i\uparrow} - \frac{1}{2} \right) \left( n_{i\downarrow} - \frac{1}{2} \right) \\
 & - \sum_i \mu_i n_i,
 \end{aligned} \tag{1}$$

where  $c_{i\sigma}$  ( $c_{i\sigma}^\dagger$ ) annihilates (creates) a fermion with spin  $\sigma$  on site  $i$ ,  $n_{i\sigma} = c_{i\sigma}^\dagger c_{i\sigma}$  is the number operator, and  $\langle \dots \rangle$  denotes nearest neighbors. We consider random onsite Coulomb interactions  $U_0 - \Delta_U < U_i < U_0 + \Delta_U$ , hopping integrals,  $t_0 - \Delta_t < t_{ij} < t_0 + \Delta_t$ , or onsite energies  $\mu_0 - \Delta_\mu < \mu_i < \mu_0 + \Delta_\mu$  drawn from a uniform distribution.  $\Delta_U$ ,  $\Delta_t$ , and  $\Delta_\mu$  are strength of disorder for the Coulomb interaction, hopping amplitude, and the onsite energy, respectively. We set  $t_0 = 1$  as the unit of energy, and except when studying the effect of  $U_0$ , keep  $U_0 = 8$  fixed throughout the paper. In any given calculation, we choose only one of the three disorder strengths to be nonzero. We work mostly with the half filled model in 2D on a simple square lattice but also study the model away from half filling and on the 3D cubic lattice with interaction and onsite energy disorders.

## III. METHODS

We use the NLCE for disordered quantum lattice models as described in detail in Ref. [51]. In the NLCE, one expresses an extensive property of the model as a series in terms of "reduced properties" associated with all connected (linked) clusters,  $c$ , that can be embedded in the

lattice  $\mathcal{L}$ ,

$$P(\mathcal{L}) = \sum_c W_P(c). \quad (2)$$

The reduced properties,  $W_P(c)$ , are in turn computed using the inclusion-exclusion principle:

$$W_P(c) = P(c) - \sum_{s \subset c} W_P(s), \quad (3)$$

where  $s$  is a cluster that can be embedded in  $c$  (a sub-cluster of  $c$ ) and  $P(c)$  is the property for the finite cluster  $c$  calculated at finite temperature exactly using full numerical diagonalization.

When  $\mathcal{L}$  represents an infinite lattice, it is more straightforward to work with the normalized quantity  $\lim_{\mathcal{L} \rightarrow \infty} P(\mathcal{L})/\mathcal{L}$  (we have taken  $\mathcal{L}$  to represent the number of sites in the lattice too). In that case, reduced properties only for those clusters not related via translational symmetry need to be included. Moreover, point group symmetries of the underlying lattice can be used to further optimize the calculations by considering a multiplicity factor and contributions from clusters that are topologically distinct and are not related through point group symmetries.

In the case of the infinite lattice, one is forced to truncate the series and include contributions from finite clusters only up to a certain size due to limitations either on the number of clusters that have to be solved or time and memory requirements for diagonalizing the largest clusters in the expansion. Therefore, in finite-temperature calculations, one typically loses convergence below a temperature where correlations in the system grow beyond the order of the largest clusters considered. This temperature depends on the model, its parameters and the order of the expansion. Details of the NLCE algorithm can be found in Ref. 50.

Here, we use the site expansion in which order  $l$  means we have included contributions from all clusters with up to  $l$  sites. Although numerical resummation algorithms can be used to extend the region of convergence of the NLCE, due to the relatively small number of terms kept in this study for the Hubbard model in the presence of disorder, we have not explored this possibility and have restricted ourselves to working with the raw expansion.

As described in Refs. 51, 54–56, the application of NLCEs can be extended to disordered systems by replacing  $P(c)$  for finite clusters in the above equations by their disorder realization averaged values. However, in Ref. 51, the authors discuss that the straightforward approach of averaging properties using randomly generated realizations may cause the NLCE to break down due to the propagation of statistical errors, unless the error bars can be driven down to the order of the machine precision [57]. Therefore, a more systematic and statistical-error-free procedure was introduced in which the limit of random disorder was approached by increasing the number of disorder modes,  $m$ , in a discrete “multi-modal”

distribution, allowing finite sums over disorder realizations to be taken exactly. It was found that with an efficient choice of mode locations in the box distribution, the convergence in the number of disorder modes could be fast, typically achieved with  $m \lesssim 6$  at the lowest temperatures the NLCE converges [51].

Here, we adopt the same algorithm and apply the method to the disordered Fermi-Hubbard models to obtain exact finite-temperature results for the thermodynamic quantities in the limit of an infinite lattice. To compare our results with those obtained via DQMC simulations of finite clusters, we employ the QUEST package [58] and, unless stated otherwise, average expectation values obtained on a  $10 \times 10$  periodic cluster in each case over at least a hundred random disorder realizations. The imaginary time step in DQMC is chosen to be 0.01 at  $T \geq 2$  for all  $U_0$  and 0.1 (0.05) at  $T < 2$  for  $U_0 = 4$  or 8 ( $U_0 = 16$ ). The comparison allows us to gauge any systematic errors as well as fluctuations due to the disorder that may exist in the latter. After discussing the convergence in the number of modes in the NLCE for the case of disorder in the onsite energies, we present results for a range of disorder strengths for each of the three types of disorder in the model.

## IV. RESULTS

### A. Convergence in disorder modes

We first examine the dependence of thermodynamic quantities on the number of disorder modes in the method at various temperatures. We use the average energy  $E = \langle H \rangle$ , double occupancy fraction  $D = \langle n_\uparrow n_\downarrow \rangle$ , spin correlations, heat capacity  $C_v$ , and entropy  $S$ . The latter two are calculated without performing a numerical derivation or integration, rather, by using the knowledge of the partition function ( $Z$ ) and other correlation functions, which are available in the NLCE within machine precision for a given cluster and disorder realization [59]:

$$S = \ln(Z) + \frac{\langle H \rangle - \mu \langle n \rangle}{T}, \quad (4)$$

and

$$C_v = \frac{1}{T^2} \left[ \langle \Delta H^2 \rangle - \frac{(\langle Hn \rangle - \langle H \rangle \langle n \rangle)^2}{\langle \Delta n^2 \rangle} \right], \quad (5)$$

where  $\rho = \langle n \rangle = \langle n_\uparrow + n_\downarrow \rangle$  is the average density, and  $\langle \Delta H^2 \rangle = \langle H^2 \rangle - \langle H \rangle^2$ , and similarly  $\langle \Delta n^2 \rangle = \langle n^2 \rangle - \langle n \rangle^2$ . At half filling, where  $\rho = 1$ , the expression for  $C_v$  reduces to the more familiar  $\langle \Delta H^2 \rangle / T^2$ . For magnetic properties, we study the nearest-neighbor spin correlations along  $z$ ,  $S^{zz} = \frac{1}{M} |\langle \sum_{\mathbf{r}} S_i^z S_{i+\mathbf{r}}^z \rangle|$ , where  $S^z = (n_\uparrow - n_\downarrow)/2$  and the sum runs over the  $M$  nearest neighbors of site  $i$ , and the antiferromagnetic structure factor  $S^{AF} = \langle (\sum_i \phi_i S_i^z)^2 \rangle$ , where the phase  $\phi_i$  alternates between  $\pm 1$  on neighboring sites.

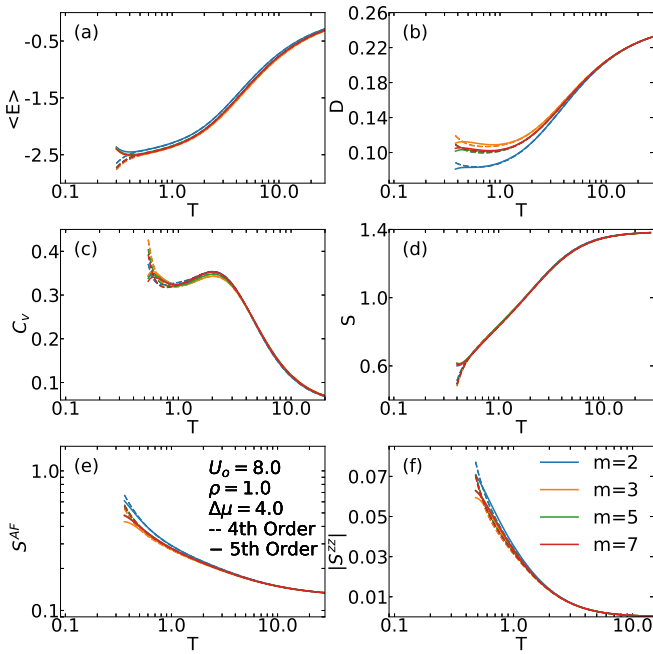


FIG. 1: NLCE results for the (a) average energy, (b) double occupancy, (c) specific heat, (d) entropy, (e) antiferromagnetic structure factor, and (f) absolute value of nearest-neighbor spin correlation vs temperature for the Hubbard model at half filling with onsite potential disorder and different number of disorder modes in the discrete distribution. The convergence of the series is lost below some temperature for the shown fourth and fifth orders, with fourth order results plotted as dashed lines and fifth order plotted as solid lines. The interaction strength is  $U_0 = 8$  and the strength of the chemical potential disorder is fixed at  $\Delta_\mu = 4$ .

Consistent with previous results for magnetic models [51], we find that the convergence of these properties with increasing the number of modes is fast, and is achieved typically with four to six modes at temperatures available to the NLCE. Figure 1 shows the results for a system at half filling ( $\mu_0 = 0$ ) and a disorder in the chemical potential with the strength  $\Delta_\mu = 4t_0$  from the fourth (dashed lines) and fifth (solid lines) orders of the NLCE. Up to seven disorder modes ( $m = 7$ ) are shown for each case. First, we observe that the NLCE for any individual  $m$  is converged generally for temperatures above  $t_0$  with the energy, entropy and the antiferromagnetic structure factor showing an extended region of convergence down to  $T \sim 0.5t_0$  for most values of  $m$ . Second, we see that the curves for  $m = 5$  and  $m = 7$  are almost indistinguishable in the temperature ranges shown for all of the quantities, except for  $C_v$  in Fig. 1(c), where significant differences persist to  $T > t_0$ . However, the results suggest that the double-peak structure in  $C_v$  survives at this disorder strength with the high-temperature peak signaling moment formation and the low-temperature peak signaling

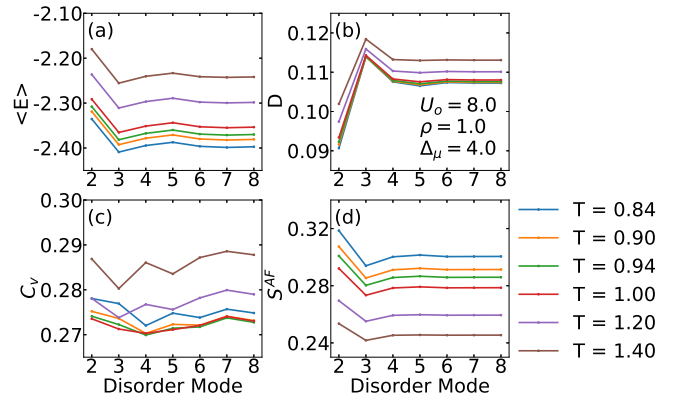


FIG. 2: Convergence in the number of disorder modes at various temperatures. Same (a) average energy, (b) double occupancy, (c) specific heat, and (d) antiferromagnetic structure factor as in Fig. 1 plotted here vs  $m$  at a few select temperatures above and below  $t_0$ . The values are from NLCE results in the fifth order.

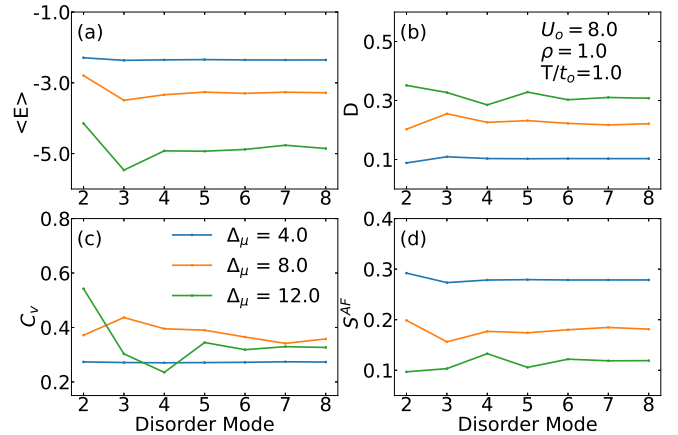


FIG. 3: Convergence in the number of disorder modes for various chemical potential disorder strengths. Same (a) average energy, (b) double occupancy, (c) specific heat, and (d) entropy as in Fig. 1 at half filling as a function of the number of disorder modes. All properties are evaluated at  $T/t_0 = 1$ , and for  $U_0 = 8$ . The values are from NLCE results in the fifth order.

moment ordering.

For the energy, the entropy and the structure factor in Figs. 1(a), 1(d), and 1(f) the convergence in  $m$  seems even faster. The fact that the double occupancy in Fig. 1(b) does not show as fast of a convergence to the continuous disorder limit at  $T < t_0$  compared to the other quantities can be understood based on the fact that double occupancy is a local quantity, and in this case, the disorder is also on local energies. As we will see later, the converged values of this property are also the most affected by increasing the strength of the disorder in the chemical potential.

Clearly, the convergence in the number of modes de-

depends on the quantity under investigation, the temperature, and as one might expect, the strength of the disorder itself. To put these in perspective, in Figs. 2 and 3, we plot four representative thermodynamic quantities from Fig. 1 as a function of  $m$  at various temperatures, or at a fixed temperature for various  $\Delta_\mu$ . Here, we have included both odd and even  $m$  up to  $m = 8$ . As one can see in Fig. 2, after relatively large initial variations from bimodal to three and four modes, most quantities quickly saturate to final values at  $T \gtrsim t_0$  while that is not the case for every quantity at  $T < t_0$  [see e.g.  $C_v$  in Fig. 2(c)]. In Fig. 3, we can see that the fluctuations in properties over different values of  $m$  increases as the disorder strength increases. Nevertheless, these results suggest that if the NLCE is converged, the approach towards the continuous disorder limit is quite fast for the energy and several other properties of the Hubbard model and can be achieved within four to six modes. Care must be taken when it comes to other properties, such as the heat capacity, when the disorder strength is relatively large. We emphasize that converged NLCE results are valid in the thermodynamic limit and do not contain any finite-size errors.

## B. Disorder in the chemical potential at half filling

Through the evolution of our thermodynamic properties upon changing the strength of the potential disorder, we find that the Hubbard system changes character when the disorder strength exceeds that of the local repulsive interaction. In Fig. 4, we show the same quantities as in Fig. 1 obtained from six orders of the NLCE for  $m = 8$  and four different values of the  $\Delta_\mu$  from 0, representing the clean system, to  $12t_0$ . Increasing  $\Delta_\mu$  causes the fraction of doubly occupied sites to increase dramatically, even beyond the uncorrelated value of  $1/4$  as the temperature decreases, while the average energy is greatly suppressed. The penalty for double occupancy is now in the range  $[U_0 - \Delta_\mu, U_0 + \Delta_\mu]$ . Therefore, a strong disorder in the chemical potential, comparable to, or larger than  $U_0$ , means having sites with a negative potential, favoring double occupancy to lower the overall energy. For weak disorder, the enhancement in double occupancy (suppression of moment formation) broadens the high-temperature peak in  $C_v$ . It is also expected to broaden the low-temperature peak as the magnetic energy scale,  $J = 4t_0^2/U_0$  for the clean system, will assume a range too [32].

The behavior is similar to what has been previously seen in QMC simulations of the disordered Hubbard model [19, 32, 60], and is also consistent with the observation that repulsive interactions larger than the disorder strength can take the system out of the disorder-induced insulating phase away from half filling [20, 33]. In the clean  $\Delta_\mu = 0$  limit, Qin *et al.* [61] find ground-state double occupancy values extrapolated to the thermodynamic limit that are in close agreement with our NLCE results

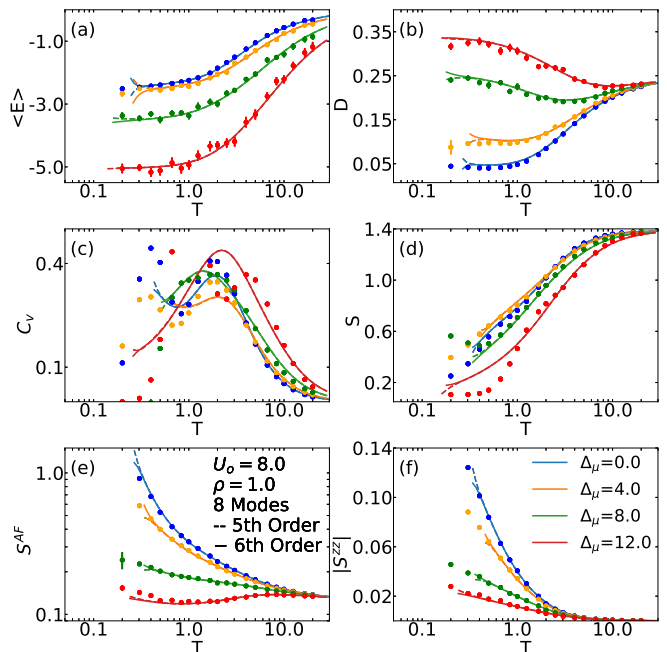


FIG. 4: Comparison of NLCE results for various chemical potential disorder strengths vs temperature. Here, the same quantities as in Fig. 1 are shown for an eight-mode disordered system at half filling with an interaction strength of  $U_0 = 8$ . Shown are the fifth (dashed lines) and sixth orders (solid lines), except for the clean system, where eighth and ninth orders are used. Included are DQMC solutions denoted by colored dots. They are for a  $10 \times 10$ -site lattice and averaged over at least 100 disorder realizations. Unless shown, symbol sizes indicate an upper bound for statistical error bars in all figures. The color mapping for the disorder ranges are the same as for the NLCE solutions.

at the lowest temperatures.

In Ref. [32], it is shown that for  $U_0 = 4$ , the antiferromagnetic correlations disappear when  $\Delta_\mu \sim 10$  on a  $4 \times 4$  cluster, which is also consistent with the trends seen for the magnetic correlations in Figs. 4(e) and 4(f), as well as in Figs. 9(e) and 9(f) below ( $U_0 = 4$ ), as the disorder strength increases. We note that our NLCE results are exact and in the thermodynamic limit, apart from possibly a few percent error for  $C_v$  at the lowest temperatures shown due to the finite number of disorder modes.

For comparison, we have reproduced DQMC results for the clean and disordered systems for quantities shown in Fig. 4. The circles in Figs. 4(a), 4(b), 4(e), and 4(f) are obtained directly using DQMC for a  $10 \times 10$  lattice after averaging expectation values over at least a hundred random disorder realizations. We find a very good agreement between those and our NLCE results in the thermodynamics limit considering that there may still be some finite-size and Trotter systematic errors present in the DQMC results. We find that keeping the number of realizations fixed, the fluctuations in the DQMC data

increases as  $\Delta_\mu$  increases. It is worth pointing out that NLCE is a far more efficient method for this problem, in terms of the computational cost, than the DQMC on the  $10 \times 10$  cluster. A single run of the latter, sweeping all the temperatures shown, takes between 6,800 and 34,000 CPU hours depending on the imaginary time step, whereas the same calculations on an arbitrarily fine temperature, or even chemical potential grid, takes about 600 CPU hours using Intel E5-2680v4 processors in our computer cluster.

The circles in Figs. 4(c) and 4(d) are obtained through the following fit of the DQMC energy [62]

$$E = E_0 + \sum_{j>0} c_j e^{-j\delta/T}, \quad (6)$$

where  $E_0$ ,  $c_j$  and  $\delta$  are the fitting parameters. The specific heat is then readily available and the entropy is obtained after integration as

$$S = S_0 + E_0/T - \sum_{j>0} c_j \frac{1 - e^{-j\delta/T}}{j\delta}, \quad (7)$$

where  $S_0 = \ln 4$  is the half filling entropy per site at infinite temperature. We keep five terms in the series for the energy and perform a least-square fit using values at 20 temperatures on a logarithmic grid between  $T \sim 0.2t_0$  and  $T \sim 20t_0$ . We note that the fit, and hence, the estimate for  $C_v$  and  $S$  can be systematically improved by increasing the number of grid points in temperature and/or reducing the statistical errors by considering more disorder realizations. So, the DQMC results shown do not necessarily represent the most accurate ones that can be achieved, rather, those from typical reasonable calculations at  $T \geq 0.2t_0$ . In fact, we find it difficult to obtain good agreement between NLCE and DQMC for  $C_v$  (and also often for  $S$ ) below a temperature of the order of  $t_0$  due to poor fits to the energy, although the two methods generally agree on the trends. A counter example is the DQMC result in Fig. 4(c) suggesting a double-peak structure in  $C_v$  for  $\Delta_\mu = 12t_0$ , which is not supported by the NLCE results.

The change of character of the system as  $\Delta_\mu$  increases is visible in the transformation of the specific heat and the entropy as well. We know that  $C_v$  for the clean Hubbard model at half filling has two distinct peaks corresponding to moment formation at  $t_0 < T < U_0$  and moment ordering at  $T < t_0$  [63, 64]. The blue curve in Fig. 4(c) for the clean system clearly captures the high-temperature peak and hints at the appearance of another low-temperature peak, observed in previous NLCE studies of the clean model using higher orders in the expansion [59]. Upon the introduction of a small disorder in  $\mu$  with a strength of  $4t_0$ , the high-temperature peak loses some weight while its location remains largely unaffected; moment formation remains the dominant physics. The less prominent peak is a signal for additional structural changes in  $C_v$  appearing in the low-temperature region associated with magnetic ordering in the clean system.

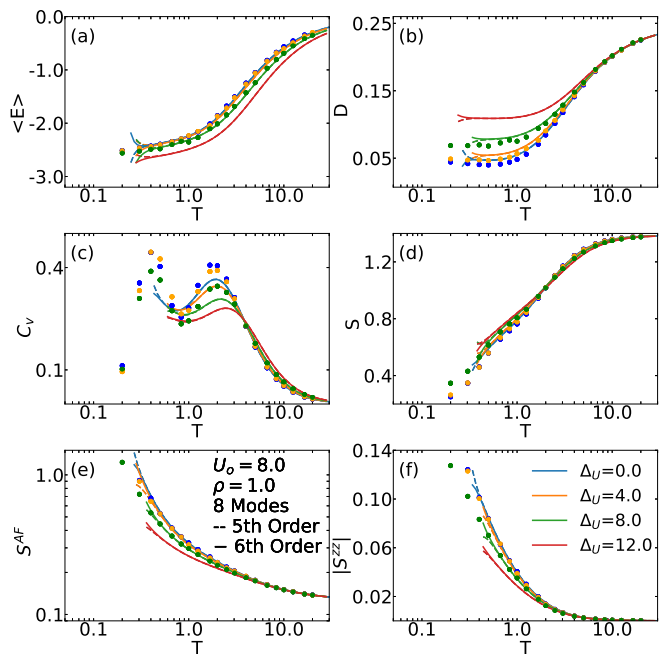


FIG. 5: Similar to Fig. 4, but for various disorder strengths in the interaction potential.

However, increasing  $\Delta_\mu$  further increases the weight for the high-temperature peak again and even creates additional weight at temperatures above the peak. For  $\Delta_\mu \gtrsim U_0$ , the peak is no longer associated with moment formation, but instead with particles localizing at sites with the lowest chemical potentials. Eventually, for a large enough  $\Delta_\mu = 12t_0$ , almost the entire weight seems to fall under one high- $T$  peak. This is also reflected in the rapid quench of the entropy at this  $\Delta_\mu$  and signals that the system is quickly settling into this phase. As can be seen in Fig. 4(e) and 4(f), any magnetic correlations are also greatly suppressed, a behavior previously shown by Ulmke et al. [65–67] and Enjalran et al. [60].

### C. Disorder in the repulsive interaction at half filling

We find that the effect of disorder in the interaction strength, which can be seen for our thermodynamic properties in Fig. 5, is less dramatic than the effect of disorder in the chemical potential. We have chosen the same four values for  $\Delta_U$  as for  $\Delta_\mu$  in Fig. 4. We find that the double occupancy retains its character for  $\Delta_U$  as large as  $12t_0$ ; decreasing as the temperature decreases. However, its low-temperature values steadily increase as  $\Delta_U$  increases as a result of roughly half of the sites having a smaller penalty for double occupancy than in the clean system. For  $\Delta_U > U_0$ , a fraction of sites are even expected to favor the formation of doublons. We benchmark our results in the case of  $\Delta_U = 0, 4$ , and  $8$  against DQMC and find very good general agreements. We observe significant

fluctuations in  $D$  and  $E$  from DQMC, which we attribute to an insufficient number of disorder realizations, and a systematic deviation from the exact NLCE results in  $D$  at low temperatures for DQMC, beyond the statistical error bars, which we attribute to the systematic Trotter error in the latter [see Figs. 5(a) and 5(b)]. The latter can be mitigated through extrapolation in the imaginary time step. We note that DQMC calculations for  $\Delta_U > 8$  run into technical difficulties as the interaction can take a negative sign (become attractive) on some sites, and so the corresponding results have not been obtained.

Similarly to the case of disorder in the local potential, the energy also decreases, yet less rapidly, upon increasing  $\Delta_U$ , here as a result of reduced repulsive, or attractive, interactions on sites that are most likely to be doubly occupied. The heat capacity and the entropy in Figs. 5(c) and 5(d) see relatively minor changes upon the introduction of the interaction disorder. The peak in  $C_v$  broadens and moves to slightly higher temperatures with increasing  $\Delta_U$ , reflecting favoring of doublons and reduction in moment formation in comparison to the clean system. At lower temperatures, the peak associated with moment ordering is also expected to broaden since disorder in interaction directly results in disorder in  $J$ . The magnetic correlations [see Figs. 5(e) and 5(f)] are suppressed with  $\Delta_U$ , especially when  $\Delta_U > 4$  as a result of having less moments available for ordering. We do not find  $\Delta_U$  affecting the convergence of the NLCE in significant ways for any of the properties we have studied.

#### D. Disorder in the hopping amplitude at half filling

We have also considered the model with bond disorder (disorder in the hopping integral  $t$ ). As can be seen in Fig. 6, in this case, the convergence of the series worsens substantially as the disorder strength increases. We attribute this to the non-local nature of this type of disorder and the sensitivity of the NLCE's performance to the variation in the non-local correlations of the system. However, already at high temperatures results point to interesting physics. Like in the case of chemical potential disorder, here the bond disorder lowers the energy dramatically, but the double occupancy does not increase as dramatically as in the former case at intermediate and low temperatures, as can be seen in Figs. 6(a) and 6(b). This can be explained through the increased tendency to form singlets on strong bonds that experience larger hoppings as the disorder increases, consistent with the observations about the magnetic behavior of the system (see below). Similar to the case of chemical potential disorder, the faster initial drop in the entropy [Fig. 6(d)] and the sign of increase in the high-temperature peak of the heat capacity [Fig. 6(c)], taking up much of the weight as the disorder increases, also capture the change in physics of the system, in this case even for disorder strengths as small as  $\Delta_t = 1.6$ . Interestingly, for the bond disorder strengths we have used, we do not see large statistical

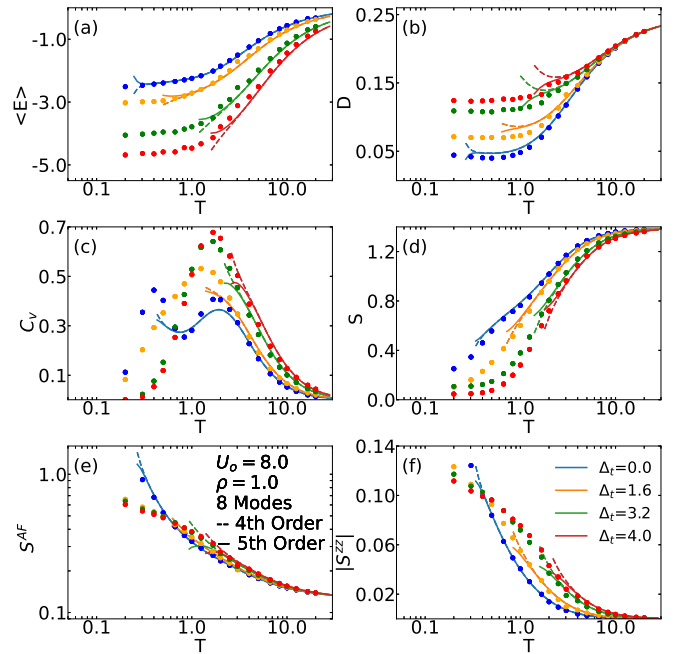


FIG. 6: Similar to Fig. 4, but for various disorder strengths in the hopping integral.

errors in the DQMC results, which prove very useful in completing the picture for the thermodynamics of the system.

The above observations are consistent with the picture drawn by the magnetic correlations shown in Figs. 6(e) and 6(f); while short-range correlations get an early boost upon lowering the temperature when the disorder strength increases, the antiferromagnetic structure factor, which encompasses long-range correlations, does not experience a big enhancement. The behavior of  $S^{zz}$  is unlike that for the system with onsite potential or interaction disorder. The latter are detrimental to any type of magnetic correlations, whereas hopping disorder can offer weak and strong bonds, favoring singlet formation on the strong bonds at the expense of long-range order in the ground state. For this reason, we expect that in the presence of sufficiently strong bond disorder  $S^{AF}$  will saturate at low temperatures. In Ref. [66], DQMC results for  $U_0 = 4$  show that the normalized structure factor at  $T = 0.1t_0$  approaches its uncorrelated value on a  $10 \times 10$  cluster for  $\Delta_t \sim 1.5$ .

#### E. Away from half filling

Our method can access thermodynamic properties and correlations functions of the system in the thermodynamic limit not only at half filling, but also all the other densities in a single run. Choosing a fine grid for the chemical potential allows for the numerical conversion to fixed densities for disordered systems after the average over realizations is performed. Here, we present results

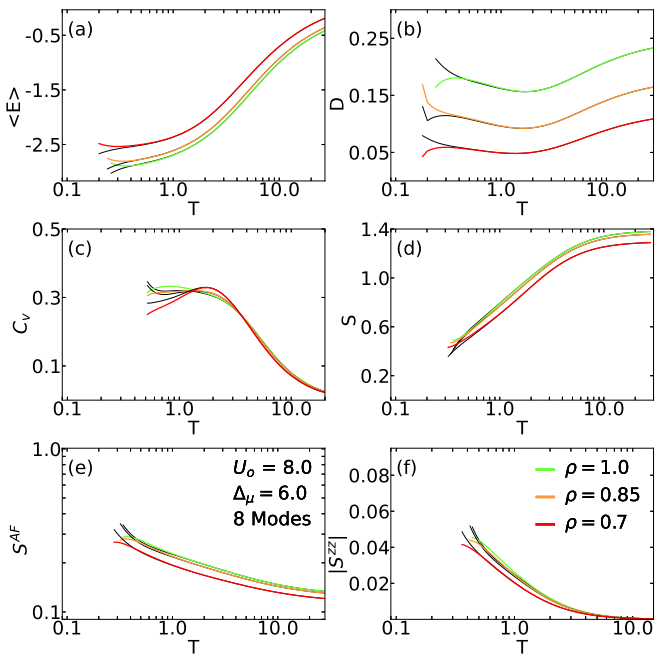


FIG. 7: Same properties as in Fig. 4, but at a fixed  $\Delta_U = 6$  away from half filling. Fourth order solutions are presented as black lines and fifth order as colored.

away from half filling for the two cases of  $\Delta_U = 6$  and  $\Delta_U = 6$  in Figs. 7 and 8. They are similar to Figs. 4 and 5, except that we have fixed  $\Delta_U$  and shown results at fixed densities of  $\rho = 1.00, 0.85$  and  $0.70$  in them.

### 1. Chemical potential disorder

The convergence of the NLCE properties for the clean Hubbard model away from half filling is typically lost at higher temperatures than can be achieved at half filling [68–71]. However, for the disordered systems, we observe that away from half filling, this temperature is comparable to, or even lower than, the lowest convergence temperature at half filling. With the onsite energy disorder (Fig. 7), we do not find significant changes in the behavior of the quantities as the disordered system with already suppressed magnetic correlations is doped away from half filling. However, there is a notable drop in the fraction of doubly occupied sites upon decreasing the density, which can be expected since having fewer particles directly translates to fewer double occupancies [68, 69]. This effect is reflected in the energy, and in turn in the  $C_v$ , which starts to develop a high-temperature peak when  $\rho = 0.7$ . The peak is close in height and location to that observed for the clean system at the same filling [72] and shows that effects of moderate site disorder at high temperature are likely minimal for the dilute system. The magnetic correlations are also slightly weakened as a result of fewer number of moments in the system.

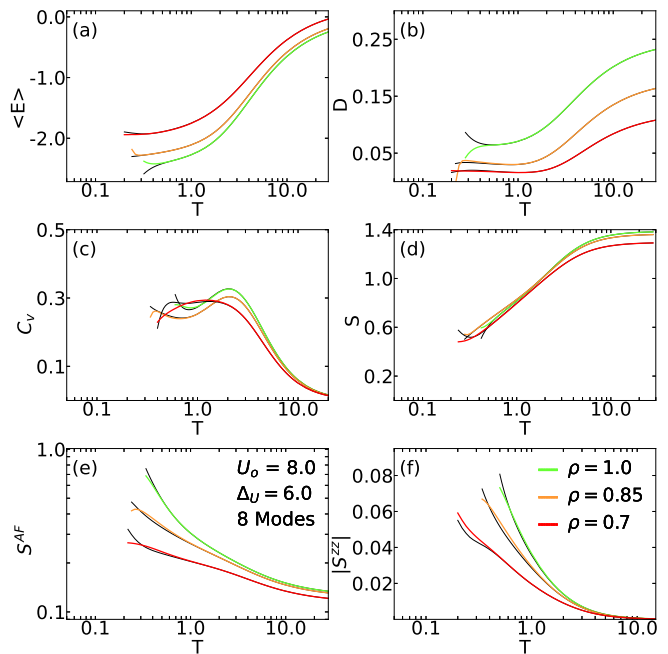


FIG. 8: Same as in Fig. 7, except for an interaction disorder of  $\Delta_U = 6$ .

We are not showing comparisons to DQMC results away from half filling since the combination of the fermion “sign problem” [73, 74] and the presence of disorder are expected to introduce large error bars at temperatures lower than  $t_0$ , especially around  $\rho = 0.875$ , also complicating the search for the average chemical potentials as a function of temperature that would yield the correct fixed densities. That would be beyond the scope of our work given that we have already established the general agreement of our NLCE results with those of DQMC for finite clusters at half filling. It also displays an advantage of using the NLCE; exact information about all fillings are readily available after a single run. In fact, such exact results in the thermodynamic limit for the disordered Fermi-Hubbard model away from half filling, while missing from the literature to the best of our knowledge, are often necessary for characterization of fermionic systems in optical lattices since the existence of the trapping potential leads to a range of densities.

### 2. Interaction disorder

A disorder in interactions with the same strength seems to have a more dramatic effect on the system and its correlations away from half filling (see Fig. 8). An already suppressed double occupancy at half filling is further reduced upon doping, and unlike the case of disorder in the onsite energies, here, doping to 30% seems to change the high-temperature character of the specific heat from that displaying clear charge peak to one in which the suppression of charge and spin degrees of freedom seems



intertwined.

We saw in Fig. 5 that the half-filled system is affected considerably less due to the interaction disorder in comparison to disorder in the chemical potential. However, Fig. 8(e) and 8(f) show that the magnetic structure factor and nearest-neighbor correlations quickly give up this resistance to change with a finite  $\Delta_U$  upon doping, leading to values at  $\rho = 0.7$  that are close to those obtained in Fig. 7 for a finite  $\Delta_\mu$ , even at half filling.

### F. Chemical potential disorder at other interaction strengths

To study the effect of site disorder on the system at other interaction strengths, we carry out calculations for the disorder in the chemical potential for  $U_0 = 4.0$  and 16.0 too. These interaction strengths represent the weak-coupling and the very strongly interacting regions of the clean model, respectively. Results are shown in Figs. 9 and 10. When  $U_0 = 4.0$ , the Coulomb repulsion and the effective nearest-neighbor exchange interaction at half filling,  $J \sim 4t_0^2/U_0$ , are of the same order of magnitude. For smaller  $U_0$ , not only other higher-order terms may have to be taken into account, but also the formation of well-defined moments in the clean system is largely hindered [63]. This is exacerbated in the presence of weak disorder, as can be inferred from the trend in the double occupancy in Fig. 9(b).

We find that many of the trends we observed in the thermodynamic properties for  $U_0 = 8.0$  upon the introduction of disorder in the chemical potential in Fig. 4 extend to other values of  $U_0$  as well. Most notably, the fact that the system behaves qualitatively differently as the temperature is lowered when the strength of the disorder reaches and exceeds the interaction strength, e.g.,  $D$  increasing with  $T$ , the suppression of magnetic correlations, etc. With  $U_0 = 16.0$  in Fig. 10(c), we can also clearly observe that the evolution of the specific heat as a function of temperature with increasing the disorder strength follows the same trends as in  $U_0 = 8.0$ . That is, the high-temperature peak initially takes less of the overall weight as  $\Delta_\mu$  increases, and as  $\Delta_\mu$  passes  $U_0$ ,  $C_v$  displays one broad high-temperature peak, signaling the onset of particles settling at low energy sites.

We note that, as has been established before for clean systems [59], NLCE appears to generally converge to lower temperatures as the interaction strength increases for the disordered system. As can be seen in Fig. 10(c), more of the nontrivial trends near the low-temperature peak of  $C_v$  can be recovered in the NLCE results when  $U_0 = 16.0$  compared to when  $U_0 = 8.0$  in Fig. 4(c). In turn, the convergence is lost at higher temperatures for  $U_0 = 4.0$  in Fig. 9(c) and NLCE does poorly even with the high-temperature peak of  $C_v$  when  $\Delta_\mu < 6.0$ . On the other hand, DQMC, while often yielding reliable results at lower temperatures than what NLCE can access for  $U_0 = 4.0$ , does poorly for  $U_0 = 16.0$ , especially for larger

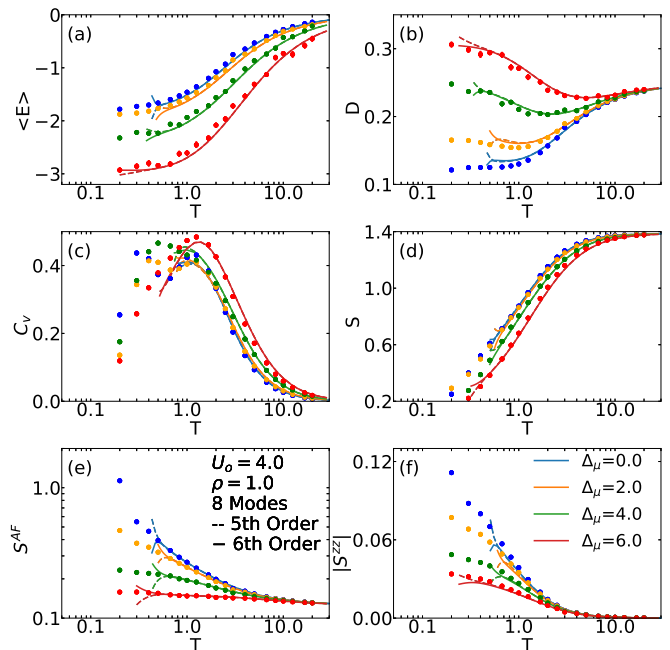


FIG. 9: Same as Fig. 4, but for  $U_0 = 4.0$ . We have taken the disorder average in DQMC (circles) over 50 realizations in this case.

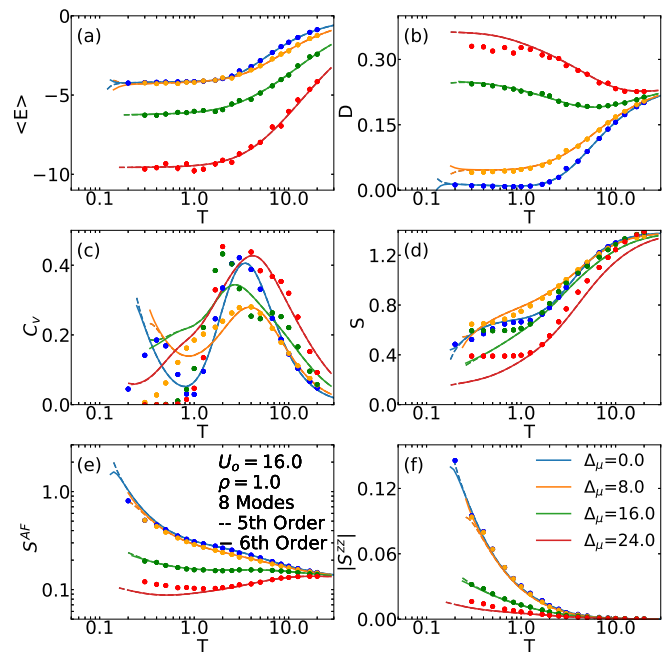


FIG. 10: Same as Fig. 9, but for  $U_0 = 16.0$ .

values of  $\Delta_\mu$ ; other than for the energy [Fig. 10(a)], the trends seen in DQMC results for thermodynamic quantities at  $T \lesssim 1.0$  when  $\Delta_\mu = 24$  in Fig. 10 cannot be trusted as they significantly deviate from converged NLCE results. That is despite reducing the Trotter error and pushing the calculations to our computational limit in

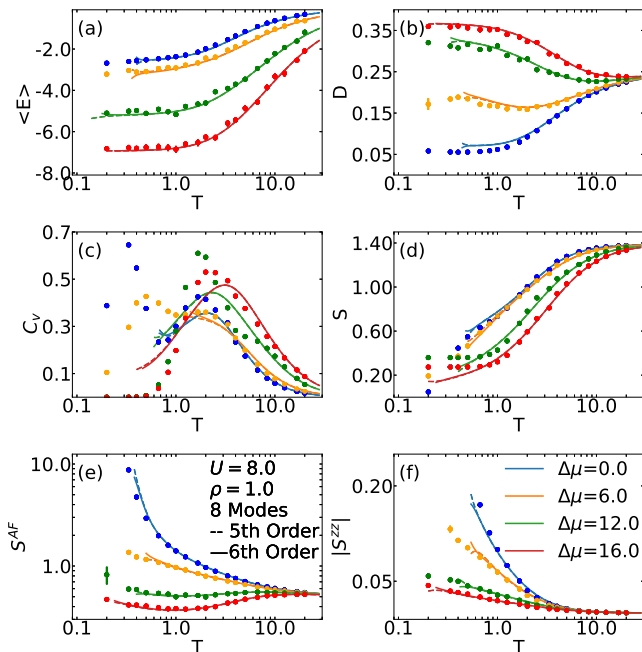


FIG. 11: Same as Fig. 4, but for the 3D version of the Fermi-Hubbard model. Symbols represent DQMC results for a  $6 \times 6 \times 6$  system.

this case. The same can be said about the specific heat and the entropy for any nonzero  $\Delta_\mu$  when  $U_0 = 16.0$  [Figs. 10(c) and 10(d)]. Hence, the results in Figs. 9 and 10 demonstrate the complementarity of the NLCE and DQMC methods, extended to disordered Hubbard systems.

### G. Chemical potential and interaction disorders in the 3D Hubbard model

By implementing our disorder averaging scheme in the 3D adaptation of the NLCE algorithm [22, 71], we have also explored the effect of disorder in the chemical potential or the interaction strength on the thermodynamic properties of the model in 3D.

In Fig. 11, we show the same properties for the 3D model that are shown for the 2D version in Fig. 4 when disorder is present in the chemical potential for a range of strengths. Here, this range is extended to  $\Delta_\mu = 16t_0$  since the noninteracting bandwidth is larger in 3D. We find that the trends are similar to those seen for the system in 2D, except that the magnetic correlations in the clean system show a more rapid increase with lowering the temperature and in turn, are affected more strongly by disorder. The divergent behavior of  $S^{AF}$  for the clean system in Fig. 11(e) reflects the existence of a finite temperature magnetic transition to the Néel phase around  $T = 0.35t_0$  for this interaction strength [71, 75]. Comparisons to DQMC results are performed considering a  $6 \times 6 \times 6$  periodic system for the latter.

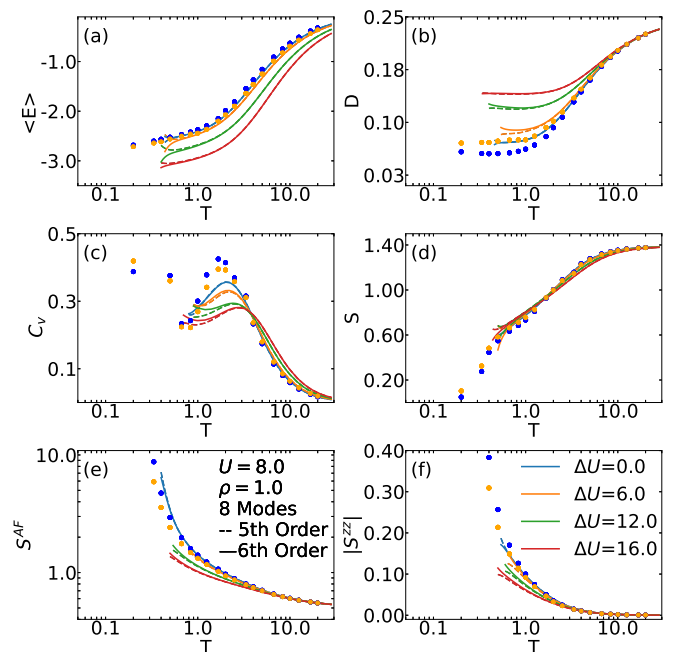


FIG. 12: Same as Fig. 11, except that the disorder is in the interaction strength.

In Fig. 12, we present results for the effect of the interaction disorder on the 3D system and find that the same trends we observed for the 2D system largely hold here as well; despite a reduction in moments in the disordered system, leading to smaller magnetic correlations, the effect of this type of disorder is much less severe, and does not appear to alter the physics of the system at temperatures we can access, in comparison to the effect of disorder in the chemical potential. Similarly to the 2D case, we cannot carry out the DQMC calculations for  $\Delta_U > 8t_0$  due to technical reasons related to the algorithm. These results show the robustness of the NLCE method for studying a wide range of circumstances that include changes in the model parameters and dimensionality of the system.

## V. SUMMARY AND DISCUSSION

In summary, we have applied the extension of the NLCE method for studying exact finite-temperature properties of disordered quantum lattice models to perform a systematic study of thermodynamic properties of the disordered Fermi-Hubbard models in two and three dimensions. We consider three different disorder scenarios involving the local chemical potential, the on-site interaction strength, and the hopping amplitude and monitor the evolution of finite-temperature properties as the strength of the disorder is increased. Among other things, we present arguments, based on the trends seen in the heat capacity, double occupancy fraction and spin correlations, about the affect of disorder on magnetic

correlations and localization effects in the system. We demonstrate that the results can be reliably extended to incommensurate fillings. We further compare our results at half filling with those obtained using the DQMC algorithm after disorder realization averaging, gauging various systematic and statistical errors in the latter as well as the temperature limitations of the NLCE in different regions.

We find that the half-filled system changes its character from moment formation and ordering as the temperature is decreased to particles localizing at sites with the lowest energies when the chemical potential disorder strength exceeds that of the local repulsive interaction. This trend persists in the weak- and strong-coupling regions as well as in 3D. The effect of bond disorder is also dramatic, and is driven by the formation of singlets on strong bonds. However, NLCE's performance is significantly affected in that case and we cannot access low temperatures. Disorder in the interaction, on the other hand, shows relatively small change in the physics of the system even for strong disorder strengths, a behavior we observe in both 2D and 3D.

The algorithm adopted here, enabling the treatment of disorder within the NLCE can be combined with the implementation of real-time correlations functions in the NLCE for systems at equilibrium to calculate dynamical properties, as were done in Refs. [29, 76], or other implementations for nonequilibrium dynamics after a quench [77–84], to extend the study of those dy-

namical properties to disordered quantum lattice models and make better connections to optical lattice experiments [21]. These experiments have so far operated at elevated temperatures ranging from  $2t_0$  to tens of  $t_0$ , well within the region of convergence of the NLCE. Moreover, our results, generally available at an order of magnitude lower temperatures, will be useful for future experiments.

In general, in optical lattice experiments aiming to emulate the disordered Fermi-Hubbard model, such as those mentioned in the introduction, disorder unavoidably manifests itself simultaneously in the on-site potential, the interaction strength, and the hopping amplitude, model parameters that already lack homogeneity over the sample due to the presence of the confining potential. This poses great challenges for parametrizing the experiments through comparisons to theoretical results and exposes the need for further development of reliable and unbiased numerical methods to meet those challenges.

## ACKNOWLEDGMENTS

We thank Richard T. Scalettar for insightful discussions. This work was supported by the National Science Foundation (NSF) under Grant No. DMR-1918572. Computations were performed on Spartan high-performance computing facility at San José State University, which is supported by the NSF under Grant No. OAC-1626645.

- 
- [1] G. A. Thomas, M. Capizzi, F. DeRosa, R. N. Bhatt, and T. M. Rice, *Phys. Rev. B* **23**, 5472 (1981).
- [2] S. V. Kravchenko, G. V. Kravchenko, J. E. Furneaux, V. M. Pudalov, and M. D'Iorio, *Phys. Rev. B* **50**, 8039 (1994).
- [3] A. Punnoose and A. M. Finkel'stein, *Science* **310**, 289 (2005), <https://science.sciencemag.org/content/310/5746/289.full.pdf>.
- [4] S. Anissimova, S. V. Kravchenko, A. Punnoose, A. M. Finkel'stein, and T. M. Klapwijk, *Nature Physics* **3**, 707 (2007).
- [5] For a review of early theoretical studies and a ground state analysis in the context of the disordered 2D two-band systems see Z. ulácsi, *Phys. Rev. B* **69**, 054204 (2004) and references therein.
- [6] W. Fu and S. Sachdev, *Phys. Rev. B* **94**, 035135 (2016).
- [7] M. Leroux, V. Mishra, J. P. C. Ruff, H. Claus, M. P. Smylie, C. Opagiste, P. Rodière, A. Kayani, G. D. Gu, J. M. Tranquada, W.-K. Kwok, Z. Islam, and U. Welp, *Proceedings of the National Academy of Sciences* **116**, 10691 (2019).
- [8] S.-H. Lee, H. Kikuchi, Y. Qiu, B. Lake, Q. Huang, K. Habicht, and K. Kiefer, *Nat Mater* **6**, 853 (2007).
- [9] F. Bert, S. Nakamae, F. Ladieu, D. L'Hôte, P. Bonville, F. Duc, J.-C. Trombe, and P. Mendels, *Phys. Rev. B* **76**, 132411 (2007).
- [10] I. Bloch, J. Dalibard, and W. Zwerger, *Rev. Mod. Phys.* **80**, 885 (2008).
- [11] J. Billy, V. Josse, Z. Zuo, A. Bernard, B. Hambrecht, P. Lugan, D. Clement, L. Sanchez-Palencia, P. Bouyer, and A. Aspect, *Nature* **453**, 891 (2008).
- [12] G. Roati, C. D'Errico, L. Fallani, M. Fattori, C. Fort, M. Zaccanti, G. Modugno, M. Modugno, and M. Inguscio, *Nature* **453**, 895 (2008).
- [13] J. E. Lye, L. Fallani, M. Modugno, D. S. Wiersma, C. Fort, and M. Inguscio, *Phys. Rev. Lett.* **95**, 070401 (2005).
- [14] S. Aubry and G. Andre, *Ann. Israel Phys. Soc.* **3**, 133 (1980).
- [15] B. Gadway, D. Pertot, J. Reeves, M. Vogt, and D. Schneble, *Phys. Rev. Lett.* **107**, 145306 (2011).
- [16] M. White, M. Pasienski, D. McKay, S. Q. Zhou, D. Ceperley, and B. DeMarco, *Phys. Rev. Lett.* **102**, 055301 (2009).
- [17] M. Pasienski, D. McKay, M. White, and B. DeMarco, *Nat Phys* **6**, 677 (2010).
- [18] M. Schreiber, S. S. Hodgman, P. Bordia, H. P. Lüschen, M. H. Fischer, R. Vosk, E. Altman, U. Schneider, and I. Bloch, *Science* **349**, 842 (2015), <http://www.sciencemag.org/content/349/6250/842.full.pdf>.
- [19] T. Paiva, E. Khatami, S. Yang, V. Rousseau, M. Jarrell, J. Moreno, R. G. Hulet, and R. T. Scalettar, *Phys. Rev. Lett.* **115**, 240402 (2015).
- [20] S. S. Kondov, W. R. McGehee, W. Xu, and B. DeMarco, *Phys. Rev. Lett.* **114**, 083002 (2015).

- [21] W. Morong, S. R. Muleady, I. Kimchi, W. Xu, R. M. Nandkishore, A. M. Rey, and B. DeMarco, *Phys. Rev. Research* **3**, L012009 (2021).
- [22] R. A. Hart, P. M. Duarte, T. L. Yang, X. Liu, T. Paiva, E. Khatami, R. T. Scalettar, N. Trivedi, D. A. Huse, and R. G. Hulet, *Nature* **519**, 211 (2015).
- [23] M. F. Parsons, A. Mazurenko, C. S. Chiu, G. Ji, D. Greif, and M. Greiner, *Science* **353**, 1253 (2016).
- [24] L. W. Cheuk, M. A. Nichols, K. R. Lawrence, M. Okan, H. Zhang, E. Khatami, N. Trivedi, T. Paiva, M. Rigol, and M. W. Zwierlein, *Science* **353**, 1260 (2016).
- [25] P. T. Brown, D. Mitra, E. Guardado-Sanchez, P. Schauß, S. S. Kondov, E. Khatami, T. Paiva, N. Trivedi, D. A. Huse, and W. S. Bakr, *Science* **357**, 1385 (2017).
- [26] A. Mazurenko, C. S. Chiu, G. Ji, M. F. Parsons, M. Kanász-Nagy, R. Schmidt, F. Grusdt, E. Demler, D. Greif, and M. Greiner, *Nature* **545**, 462 (2017).
- [27] C. S. Chiu, G. Ji, A. Mazurenko, D. Greif, and M. Greiner, *Phys. Rev. Lett.* **120**, 243201 (2018).
- [28] P. T. Brown, D. Mitra, E. Guardado-Sanchez, R. Nourafkan, A. Reymbaut, C.-D. Hébert, S. Bergeron, A.-M. S. Tremblay, J. Kokalj, D. A. Huse, P. Schauß, and W. S. Bakr, *Science* **363**, 379 (2019).
- [29] M. A. Nichols, L. W. Cheuk, M. Okan, T. R. Hartke, E. Mendez, T. Senthil, E. Khatami, H. Zhang, and M. W. Zwierlein, *Science* **363**, 383 (2019).
- [30] M. Gall, N. Wurz, J. Samland, C. F. Chan, and M. Köhl, *Nature* **589**, 40 (2021).
- [31] R. Blankenbecler, D. J. Scalapino, and R. L. Sugar, *Phys. Rev. D* **24**, 2278 (1981).
- [32] M. Ulmke, P. J. H. Denteneer, V. Janiš, R. T. Scalettar, A. Singh, D. Vollhardt, and G. T. Zimanyi, in *Advances in Solid State Physics 38*, edited by B. Kramer (Springer Berlin Heidelberg, Berlin, Heidelberg, 1999) pp. 369–381.
- [33] P. J. H. Denteneer, R. T. Scalettar, and N. Trivedi, *Phys. Rev. Lett.* **83**, 4610 (1999).
- [34] D. Heidarian and N. Trivedi, *Phys. Rev. Lett.* **93**, 126401 (2004).
- [35] K. Bouadim, Y. L. Loh, M. Randeria, and N. Trivedi, *Nat Phys* **7**, 884 (2011).
- [36] E. Lahoud, O. N. Meetei, K. B. Chaska, A. Kanigel, and N. Trivedi, *Phys. Rev. Lett.* **112**, 206402 (2014).
- [37] A. Mukherjee, N. D. Patel, S. Dong, S. Johnston, A. Moreo, and E. Dagotto, *Phys. Rev. B* **90**, 205133 (2014).
- [38] S. R. White, *Phys. Rev. Lett.* **69**, 2863 (1992).
- [39] J. Wernsdorfer, G. Harder, U. Schollwoeck, and W. Hofstetter, (Unpublished) preprint: arXiv:1108.6057 (2011).
- [40] A. Georges, G. Kotliar, W. Krauth, and M. J. Rozenberg, *Rev. Mod. Phys.* **68**, 13 (1996).
- [41] M. H. Hettler, A. N. Tahvildar-Zadeh, M. Jarrell, T. Pruschke, and H. R. Krishnamurthy, *Phys. Rev. B* **58**, R7475 (1998).
- [42] V. Dobrosavljević and G. Kotliar, *Phys. Rev. Lett.* **78**, 3943 (1997).
- [43] M. V. Sadovskii, I. A. Nekrasov, E. Z. Kuchinskii, T. Pruschke, and V. I. Anisimov, *Phys. Rev. B* **72**, 155105 (2005).
- [44] E. Z. Kuchinskii and M. V. Sadovskii, *Journal of Experimental and Theoretical Physics* **122**, 509 (2015).
- [45] C. E. Ekuma, H. Terletska, K.-M. Tam, Z.-Y. Meng, J. Moreno, and M. Jarrell, *Phys. Rev. B* **89**, 081107(R) (2014).
- [46] H. Terletska, C. E. Ekuma, C. Moore, K.-M. Tam, J. Moreno, and M. Jarrell, *Phys. Rev. B* **90**, 094208 (2014).
- [47] R. Kotlyar and S. Das Sarma, *Phys. Rev. Lett.* **86**, 2388 (2001).
- [48] R. Mondaini and M. Rigol, *Phys. Rev. A* **92**, 041601(R) (2015).
- [49] M. Rigol, T. Bryant, and R. R. P. Singh, *Phys. Rev. Lett.* **97**, 187202 (2006).
- [50] B. Tang, E. Khatami, and M. Rigol, *Computer Physics Communications* **184**, 557 (2013).
- [51] M. D. Mulanax, D. Almada, and E. Khatami, *Phys. Rev. B* **99**, 205113 (2019).
- [52] N. F. Mott, *Proceedings of the Physical Society. Section A* **62**, 416 (1948).
- [53] J. Hubbard, *Proceedings of the Royal Society of London A: Mathematical and Physical Sciences* **276**, 238 (1954).
- [54] R. R. P. Singh and S. Chakravarty, *Phys. Rev. Lett.* **57**, 245 (1986).
- [55] B. Tang, D. Iyer, and M. Rigol, *Phys. Rev. B* **91**, 161109(R) (2015).
- [56] B. Tang, D. Iyer, and M. Rigol, *Phys. Rev. B* **91**, 174413 (2015).
- [57] T. Devakul and R. R. P. Singh, *Phys. Rev. Lett.* **115**, 187201 (2015).
- [58] Codes available at <http://quest.ucdavis.edu/> and <https://code.google.com/p/quest-qmc>.
- [59] E. Khatami and M. Rigol, *Phys. Rev. A* **86**, 023633 (2012).
- [60] M. Enjalran, F. Hébert, G. G. Batrouni, R. T. Scalettar, and S. Zhang, *Phys. Rev. B* **64**, 184402 (2001).
- [61] M. Qin, H. Shi, and S. Zhang, *Phys. Rev. B* **94**, 085103 (2016).
- [62] C. Huscroft, A. K. McMahan, and R. T. Scalettar, *Phys. Rev. Lett.* **82**, 2342 (1999).
- [63] T. Paiva, R. T. Scalettar, C. Huscroft, and A. K. McMahan, *Phys. Rev. B* **63**, 125116 (2001).
- [64] J. Bonča and P. Prelovšek, *Phys. Rev. B* **67**, 085103 (2003).
- [65] M. Ulmke, V. Janiš, and D. Vollhardt, *Phys. Rev. B* **51**, 10411 (1995).
- [66] M. Ulmke and R. T. Scalettar, *Phys. Rev. B* **55**, 4149 (1997).
- [67] M. Ulmke, P. J. H. Denteneer, R. T. Scalettar, and G. T. Zimanyi, *Europhysics Letters (EPL)* **42**, 655 (1998).
- [68] E. Khatami and M. Rigol, *Phys. Rev. A* **84**, 053611 (2011).
- [69] B. Tang, T. Paiva, E. Khatami, and M. Rigol, *Phys. Rev. B* **88**, 125127 (2013).
- [70] E. Khatami, R. T. Scalettar, and R. R. P. Singh, *Phys. Rev. B(R)* **91**, 241107(R) (2015).
- [71] E. Khatami, *Phys. Rev. B* **94**, 125114 (2016).
- [72] D. Duffy and A. Moreo, *Phys. Rev. B* **55**, 12918 (1997).
- [73] E. Y. Loh, J. E. Gubernatis, R. T. Scalettar, S. R. White, D. J. Scalapino, and R. L. Sugar, *Phys. Rev. B* **41**, 9301 (1990).
- [74] V. I. Iglovikov, E. Khatami, and R. T. Scalettar, *Phys. Rev. B* **92**, 045110 (2015).
- [75] R. Staudt, M. Dzierzawa, and A. Muramatsu, *The European Physical Journal B - Condensed Matter and Complex Systems* **2015**, 12001 (2015).
- [76] J. Richter and R. Steinigeweg, *Phys. Rev. B* **99**, 094419 (2019).
- [77] M. Rigol, *Phys. Rev. Lett.* **112**, 170601 (2014).
- [78] M. Rigol, *Phys. Rev. E* **90**, 031301(R) (2014).
- [79] B. Wouters, J. De Nardis, M. Brockmann, D. Fioretto, M. Rigol, and J.-S. Caux, *Phys. Rev. Lett.* **113**, 117202 (2014).

- [80] K. Mallayya and M. Rigol, Phys. Rev. E **95**, 033302 (2017).
- [81] K. Mallayya and M. Rigol, Phys. Rev. Lett. **120**, 070603 (2018).
- [82] I. G. White, B. Sundar, and K. R. A. Hazzard, arXiv:1710.07696 (2017).
- [83] J. Gan and K. R. A. Hazzard, Phys. Rev. A **102**, 013318 (2020).
- [84] J. Richter, T. Heitmann, and R. Steinigeweg, SciPost Phys. **9**, 31 (2020).